The behaviour of bridge abutments on spread foundations

Comportement des butées sur fondations étendues

M. D. BOLTON & H.W. SUN, Cambridge University Engineering Department, UK

ABSTRACT: Centrifuge models have revealed the modes of displacement of bridge abutments on clay retaining granular fill. Wall displacements driven by active earth pressures during backfilling are closely matched by a simple plastic deformation calculation based on the clay strength mobilized at a compatible shear strain. Consolidation generates differential settlements, but the stiff backfill prevents further lateral displacements at the crest. While collapse of the bridge deck is thereby avoided, earth pressures on the wall are increased.

RESUME: Les modèles centrifugeuses ont rèvèlé les modes du deplacement des butèes au dessus d'argile et quelles retient les remblais du sable. Les deplacements du mur, etant poussé par la pression active, sont près des calculs simples plastiques, fondé ssur la résistance mobilisé par un deformation compatible. Le consolidation produise les tassements différentiels, mais le remblais rigide prévient le déplacement latèral supplementair du sommet. Tandis que l'écroulement du pont est évité, le deformation du mur est augmenté par la poussée additionelle du remblais.

1 INTRODUCTION

As pointed out in a report of the Building Research Establishment, BRE (1979), bridge designers often try to avoid piled foundations on grounds of economy. A spread base abutment, Figure 1, can usually be constructed to suit the ground conditions on the site without the need for mobilizing heavy construction plant. Horizontal movement at the level of the bridge deck bearing was found to be the most critical criterion, and this is confirmed by a recent report from the US Department of Transport, FHWA (1985), on the performance of 314 bridges. Frequent damage to the bridge was found in abutments with horizontal movement greater than 50mm while half of the bridges experiencing 100mm differential settlement were found to be undamaged and the rest only suffered from minor cracking or minor distress. Many designers are unwilling to risk the possibility of unservicability through lateral displacement of the spread base abutment on firm to stiff clay, especially since direct calculation procedure for horizontal ground displacement is not available for this type of foundation soil. A research project was sponsored by the UK Transport and Road Research Laboratory for the investigation of an abutment wall on clay through centrifuge model tests on the balance beam centrifuge at the Cambridge University Geotechnical Centrifuge Centre. This paper describes the behaviour of the centrifuge model wall and suggests analytical approaches.

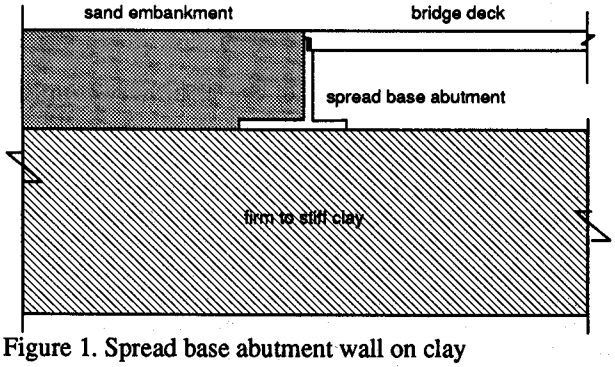

Figure 1. Spread base abutment wall on clay

2 CENTRIFUGE TESTS

Centrifuge modelling is useful in identifying soil-structure interaction at reduced scale and providing data on an idealized prototype for the development of analytical techniques. In the investigation of the interaction of a spread base abutment wall and its embankment fill on a clay foundation, five centrifuge model tests were performed on the Cambridge University 10m beam centrifuge (Schofield 1980). Figure 2 shows a typical 1/100 centrifuge model from this series of experiments on firm to stiff kaolin clay. Figure 3 presents the undrained shear strength profile of the clay foundation measured by in-flight shear vane tests in the centrifuge.

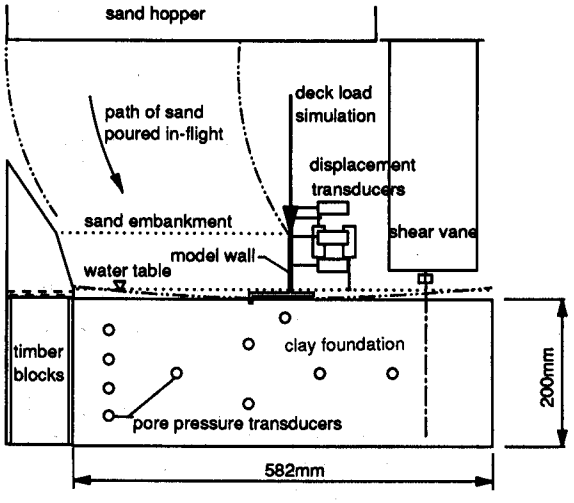

Figure 2. A typical centrifuge model

2.1 Embankment construction and immediate displacements

Sand embankment construction in the model was simulated by in-flight sand pouring from a hopper located above the model. Embankment construction caused an immediate

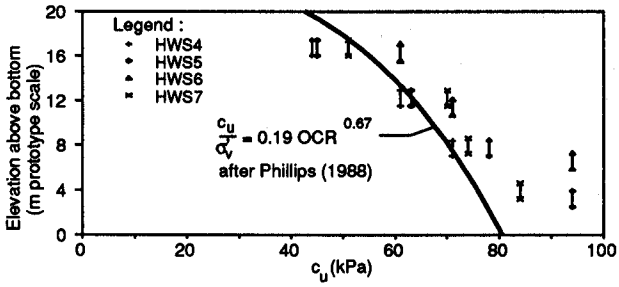

Figure 3. Undrained shear strength profile of clay foundation

heave, forward translation and backward rotation of the wall reference point. Figure 4 shows the displacements of the clay foundation just after the embankment construction was completed in test HWS3, revealed by measuring the in-flight photographs before and after sand-pouring. Forward translation of the wall causes the lateral pressure to drop to the active value mobilizing its critical shear strength. Figure 5 plots bending moments in the wall stem measured in tests HWS3 to HWS7 and the prediction by a linear pressure distribution with k_a=0.271 (ϕ=35°).

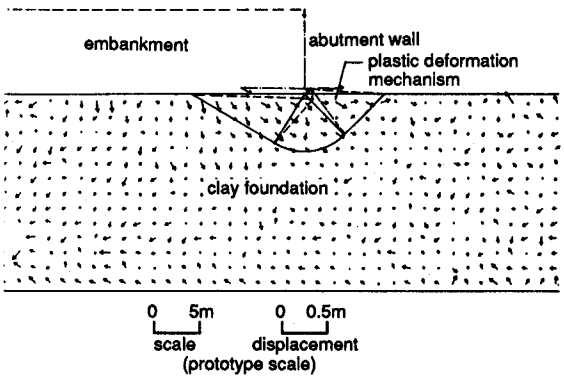

Figure 4. Undrained subsoil displacement and its prediction - test HWS3

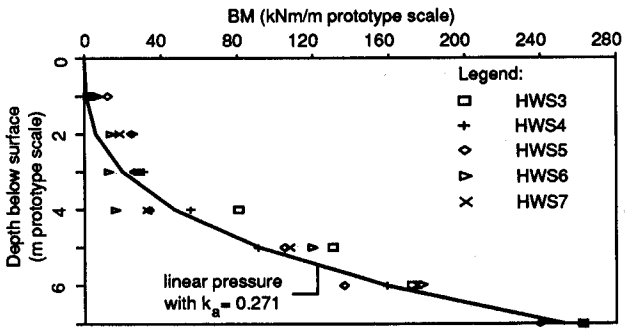

Figure 5. Bending moment on wall stem immediately after embankment building

The stress-strain response of an over-consolidated clay, which remains within the yield surface defined by its maximum consolidation pressure, is not linearly elastic. Non-linearity and anisotropy of the soil depend on the inherent anisotropy of its particle structure and the induced anisotropy of its current stress-path direction, stress and strain history.

Active and passive undrained cyclic stress path tests on vertical and horizontal plane-strain samples, as described in Sun (1990), show different stress-strain responses which reflect the strong inherent anisotropy in stiffness of the one-dimensionally consolidated kaolin, Figure 6. Strain-dependent stiffness response of the clay is also controlled by its induced anisotropy due to its immediate past strain path. Figure 7 shows the strain directions in the 5.4m thick zone of swelling overconsolidated clay in the centrifuge model. Immediately underneath the embankment in the active zone, the strain will reverse from swelling, while strain will continue from swelling in the adjacent soil of the passive zone. Shear stress-strain response can then be deduced from the directions and magnitude of immediate past shear strain and the expected directions of strains in the clay foundation, Figure 8. The re-compressed overconsolidated clay under 5.4m depth in the centrifuge prototype is expected to be on average 10 times stiffer than the swelling clay above because of the strain reversal in the very stiff passive response. Therefore, deformation is confined to shallow depths above 5.4m.

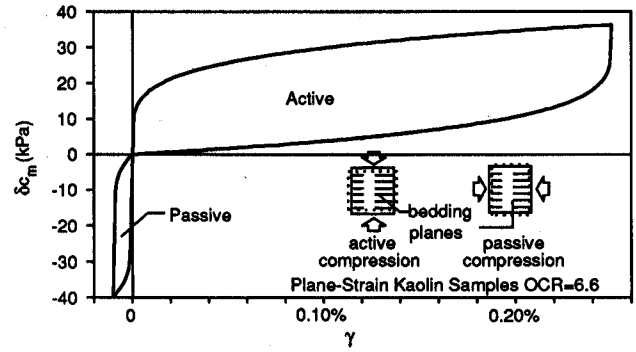

Figure 6. Undrained cyclic stress-strain response of overconsolidated kaolin

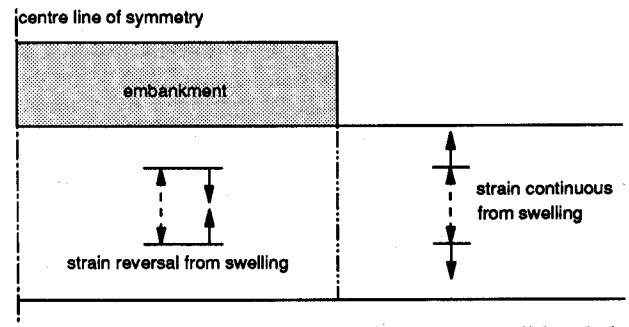

Figure 7. Strain directions in swelling overconsolidated clay under new embankment

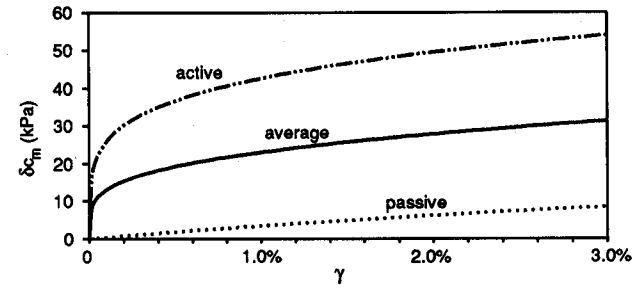

Figure 8. Stress-strain response of clay element at 2.7m below ground surface

An elementary extension to the conventional plasticity bearing capacity calculation has led to the development of a plastic deformation mechanism calculation, Sun (1990), for the estimation of undrained soil displacement under the embankment. The configuration of the plastic mechanism in undrained ground deformation is superimposed on Figure 4 for test HWS3 and Figure 9 represents the condition in test

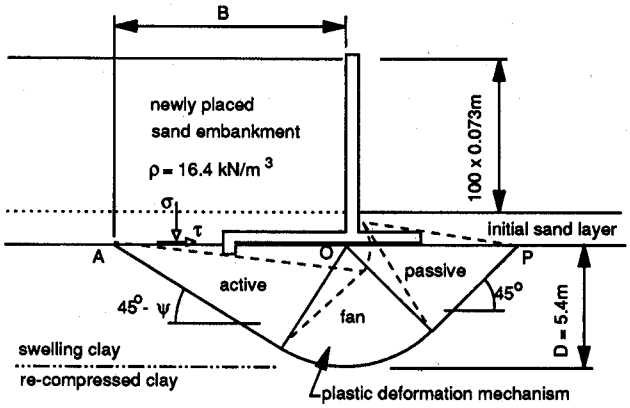

Figure 9. Undrained ground deformation for wall movement prediction - test HWS7

HWS7. It is more convenient to adopt an average stiffness response, Figure 8, in the whole mechanism, although this will cause a small equilibrium error, depending on the size of the active zone compared with the size of the whole mechanism. The equilibrium equation links the surface loading to the average additional shear strength $\delta\bar{c}_m$ mobilized within the zone of deformation:

$$\sigma = \delta\bar{c}_m + \delta\bar{c}_m\left(\pi - \sin^{-1}\frac{\tau}{\delta\bar{c}_m}\right) + \sqrt{\delta\bar{c}_m^2 - \tau^2} \qquad (1)$$

The relationship between the ratio of shear and normal stress and the angle ψ in Figure 9 is given by:

$$\frac{\tau}{\sigma} = \frac{\sin 2\psi}{1 + \pi - 2\psi + \cos 2\psi} \qquad (2)$$

The depth of the mechanism D is 5.4m, restricted to the swelling clay, and the width B of the active block can be related by:

$$D = \frac{B}{\sqrt{2}}(\cos\psi - \sin\psi) \qquad (3)$$

where $\psi = 0.5\sin^{-1}(\tau/\delta\bar{c}_m)$

The ground surface movement, Figure 10, is linked to shear strain increment γ in the active and passive zones. The ground surface movement δ_v and δ_h at the middle of width B is given by:

$$\delta_v = 0.25\gamma B(\cos\psi - \sin\psi)^2 \qquad (4)$$

$$\delta_h = 0.25\gamma B(\cos^2\psi - \sin^2\psi) \qquad (5)$$

and the movement δ'_v and δ'_h at the middle of the passive zone ground surface is related to δ_v by:

$$\frac{-\delta_v}{\delta'_v} = \frac{\delta_v}{\delta'_h} = \cos\psi + \sin\psi \qquad (6)$$

In order to balance the lateral pressure in the backfill, which is at its active state above the width B of the mechanism, the horizontal traction τ is assumed to be distributed evenly on the width B of the deformation mechanism, although shear stress from fully active backfill should only be transferred to the ground by the base of the abutment wall. For test HWS7, vertical surcharge on the width B is equal to σ = 100 x 16.4 kN/m³ x 0.073m = 120 kN/m², and the horizontal traction τ = 0.5 x k x σ x 100 x 0.073m / B = 118.7 / B kN/m² where

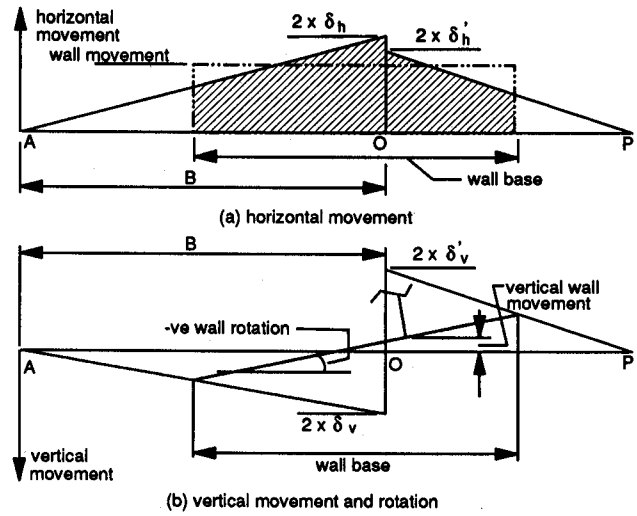

Figure 10. The estimation of wall movement from ground deformation under the base

k=0.271. Solving equations 2 and 3 together with σ and τ, angle ψ is found to be 13.12° and B is 10.22m. $\delta\bar{c}_m$ is found to be 26.2 kN/m² from equation 1, then shear strain γ = 1.6% can be read from the stress-strain diagram, Figure 8. Finally, δ_v = 0.023m, δ_h = 0.037m, δ'_v = 0.031m and δ'_h = 0.031m is calculated from equations 4 to 6.

To convert ground movements underneath the wall base into a prediction of wall movement, some simplifications were made. Horizontal movement of the wall was assumed to be the average value of the ground surface movement under the base, Figure 10(a), and no relative slippage between subsoil and wall base was expected. Rotation of the wall was calculated from the vertical ground movements of the points on the soil surface at the edges of the wall base, Figure 10(b). Vertical movement of the wall was estimated from the wall rotation and ground movement at the edges of the wall base, Figure 10(b). Figure 11 compares the prediction and the test results.

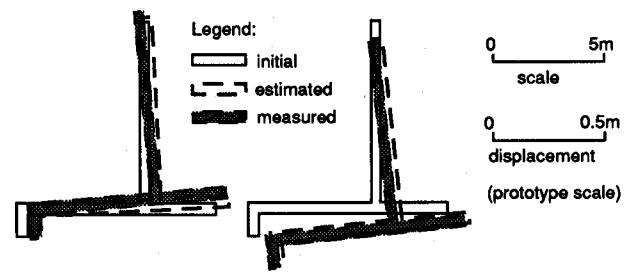

Figure 11. Wall movements in test HWS7

2.2 *Foundation consolidation and interactions*

Consolidation of the model clay foundation took place in the next 5.5 to 6 hours (6 years and 3 months to 6 years and 10 months at prototype scale). Ground displacement due to consolidation was mainly one-dimensional settlement as observed from the in-flight photographs. Figure 12 shows the incremental subsoil displacement between undrained and consolidated states in test HWS3. Pore pressure changes measured in the over-consolidated clay beneath the newly constructed embankment were found to match the prediction of an elastic solution rather closely. One dimensional settlement calculations based on the dissipation of the

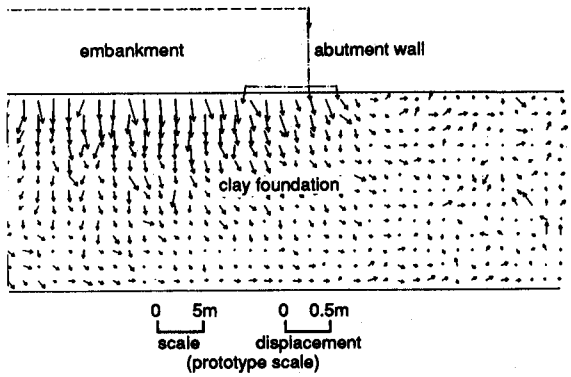

Figure 12. Subsoil displacement due to consolidation under embankment load in test HWS3

estimated pore pressure were found to agree with test results. Differential settlement at the edge of the embankment caused the wall to rotate backwards forcing the stem to press into the backfill. As the foundation clay is less stiff than the backfill in this mode of movement, the top of the wall stem remained on the same vertical plane while the base moved out. Figure 11 shows also the predicted final wall movement against the test result in test HWS7, based on the settlement profile estimation. Furthermore, the relative displacement between the backfill and the wall, which was caused by its backward rotation, induced an increase of the lateral earth pressure acting behind, Figure 13. Figure 14 shows a part of the bending moment time record of test HWS7.

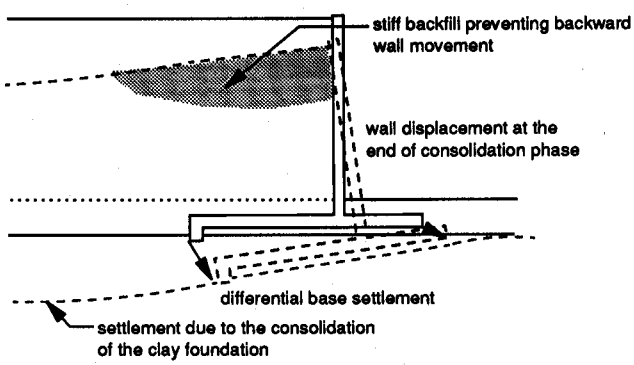

Figure 13. The interaction of the abutment wall during the consolidation of its clay foundation

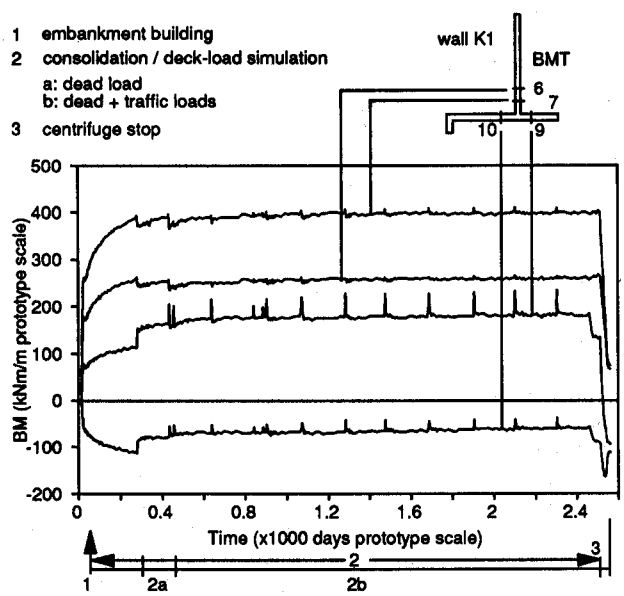

Figure 14. Bending moment time record of test HWS7

2.3 Bridge deck loadings

Vertical bridge deck loading on the wall stem was simulated after embankment construction in tests HWS5 to HWS7. It was achieved by the application of cycles of quasi-static live load superimposed on a "dead-load" base line by two pneumatic jacks located above the wall stem. It was found in the test that the first application of the "dead-load" and the first cycle of the heavy live load each caused a slight change in wall movement and bending moment on the stem, Figure 14. These effects remained after the removal of the live load but the influences of subsequent cycles of live load were insignificant, except the instantaneous response from the bending moment transducers on the wall base, Figure 14. This can be explained by the high stiffness on unloading and reloading in the clay foundation and backfill.

3 CONCLUSION

Ground deformations in centrifuge models or in the field are often more localized then those predicted by linear elastic solutions. Plastic deformation mechanisms based on the method of characteristics resembled patterns of undrained deformation in the models. Furthermore, the magnitude of undrained soil displacements has been predicted by deducing mobilized soil strengths, and relating these to shear strain increments observed in stress-path tests. The accuracy of this modified plastic approach to displacement prediction of abutment walls is apparently sufficient to form the basis of a design method.

The model walls displayed negligible displacement at the elevation of the bridge deck in the later phase of backward rotation due to consolidation beneath the new embankment. This was attributed to the relative stiffness of the backfill, in comparison with the clay foundation.

REFERENCES

Building Research Establishment. 1979. Bridge Foundations and Substructures, UK Department of Environment, HMSO.

Phillips, R. 1988. Centrifuge Lateral Piles Tests in Clay, Tasks 2 & 3, a report to Exxon Production Research Corp. by Lynxvale Ltd., Cambridge, UK.

Schofield, A.N. 1980. Cambridge University Geotechnical Centrifuge Operations, Géotechnique, 30 (3), 1980, 227-268.

Sun, H.W. 1990. Ground Deformation Mechanisms for Soil-Structure Interaction, Forthcoming PhD Dissertation, Cambridge University, UK.

U.S. Department of Transportation, 1985. Tolerable Movement Criteria for Highway Bridges. Final Report FHWA/RD-85/107, Federal Highway Administration, USA.

ACKNOWLEDGEMENTS

The work described here was supported by a research contract let by the Transport and Road Research Laboratory of the UK Department of Transport. The opinions expressed here are the authors' and do not necessary coincide with those of the Laboratory or the Department.

Wing Sun is grateful for the financial support of the Croucher Foundation of Hong Kong, and the Overseas Research Student Award from the CVCP of British Universities.